A Modified Murray-Davies Model of Halftone Gray Scales

J.S. Arney* , P.G. Engeldrum**, H. Zeng*

Abstract

An empirical model has been developed to describe tone reproduction in halftone imaging. The model is based on experimental measurements of the image microstructure of halftone grey scales produced by offset lithography, thermal transfer, and ink jet. Like the Yule-Nielsen model, which contains an arbitrary constant called the "Yule n factor", the model developed in the current study is derived from the Murray-Davies equation. However, the current model contains two empirical parameters, w and v. The w factor relates to the optical spread function of the paper relative to the spatial frequency of the halftone dots. The v factor relates to the distribution of colorant within the dot. The Yule-Nielsen model describes only the relationship between the mean reflectance, R, of the halftone image and the dot area fraction, F_i. The current model describes R versus F_i and also some experimental data on the image microstructure. With the Yule-Nielsen model, estimates of the n factor are traditionally made by fitting the model to R versus F_i data. With the current model, estimates of w and v are chosen to fit the image microstructure data. The resulting values of w and v are then found to provide an excellent fit with the mean reflectance, R, versus F_i data.

Introduction

The first optical model of tone reproduction in the halftone process was the Murray-Davies equation, first published in 1936[1] . This model describes a linear relationship between the reflectance, R, of

$$R(F_i)=F_iR_i+(1-F_i)R_p \tag{1}$$

the halftone image and the fractional area, F_i, of the printed substrate that is covered by ink. The constants R_i and R_p are the reflectance of the ink and the paper, respectively. Variation from linearity is typically observed and is often modeled with the Yule-Nielsen

$$R(F_i)=[F_iR_i^{1/n}+(1-F_i)R_p^{1/n}]^n \tag{2}$$

modification of the Murray-Davies equation, where n is an

* Center for Imaging Science, Rochester Institute of Technology
**Imcoteck

Figure 1: Reflectance histograms of ink jet halftone grey scales at (A) $F_i = 0.05$, (B) $F_i = 0.5$ and $F_i = 0.90$. Histogram frequencies, H(R), are normalized to unity for the highest peak.

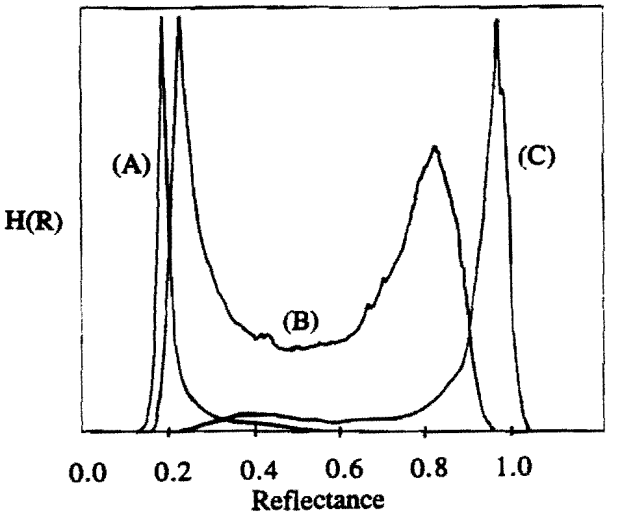

Figure 2: Ink jet halftone data at 65 LPI. Reflectance versus Dot Area Fraction, F_i , for overall reflectance $R(F_i)$, ink reflectance $R_i(F_i)$, and reflectance of paper between the dots $R_p(F_i)$. Solid lines are modeled with $w = 0.526$.

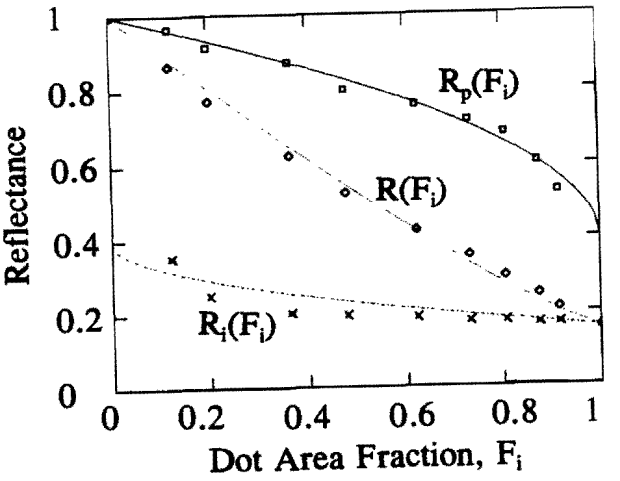

imperical constant chosen to provide a good fit to experimental data.[2,3,4,5] Experimentally it is well known that the non-linearity of R versus F_i is a manifestation of light scattering within the halftone image.[6,7,8,9] However, while excellent theoretical work has been published to derive the Yule-Nielsen expression from first principles, the Yule-Nielsen equation is found to result only from special limiting assumptions.[10,11] Moreover, the Yule-Nielsen equation would appear to be contrary to the conservation of energy since it adds reflectances raised to a power, 1/n. Reflectance is proportional to photon flux and thus should add linearly, as originally suggested by Murray-Davies.

In this report, the authors would like to suggest an alternative model that preserves the linear additivity of reflectance in the original Murray-Davies equation but accounts for the non-linearity between R and F_i. Like the Yule-Nielsen model, the new model is derived empirically from the Murray-Davies equation.

Experimental Observations of R_i and R_p

A 65 LPI halftone grey scale was generated by a Canon BJC-600, bubble-jet printer as described in the appendix. Images at each dot percent in the grey scale were captured with a CCD camera through a microscope. The camera was calibrated against known reflectance standards, so pixel values were converted to reflectance values and a reflectance distribution, or histogram, was plotted, as shown in Figure (1). The peaks in the histogram correspond to the reflectance of the ink and the paper between the dots, so from Figure (1B) we observe the average reflectance of the ink (R_i = 0.20) and the average reflectnace of the paper between the dots (R_p = 0.80). The value of the dot fraction, F_i = 0.50, also can be measured from analysis of the image microstructure, as described in the appendix. Finally, by integrating the histogram, an overall reflectance, R, of the image is obrained. Values of F_i, R_i, R_p, and R were measured in this way for each nominally printed dot percent in the grey scale. Figure (2) summarizes the observations, and it is clear that not only the mean R of the iamge, but also R_i (F_i) and $R_p(F_i)$ are functions of the dot fraction, F_i. It is evident the non-linearity observed in R versus F_i is a manifestation of the variation of R_i and R_p with F_i . Thus, it should be possable to model the dependence of the mean reflectance, R, on dot fraction, F_i, with the Murray-Davies equation provided the constant, R_i and R_p are replaced with the funcitons, $R_i(F_i)$ and $R_p(F_i)$.

$$R(F_i)=F_iR_i(F_i)+(1-F_i)R_p(R_i) \qquad (3)$$

One may test the effacacy of equation (3) as a model for halftone imaging by using experimentally measured values of F_i, $R_i(F_i)$, and $R_p(F_i)$ from the histogram, and calculating the corresponding value of the mean image reflectance, R. One may compare R with the

Figure 3: Reflectance values calculated with equation (6) using measured values of Ri, Rp, and F versus measured values of macroscopic reflectance.

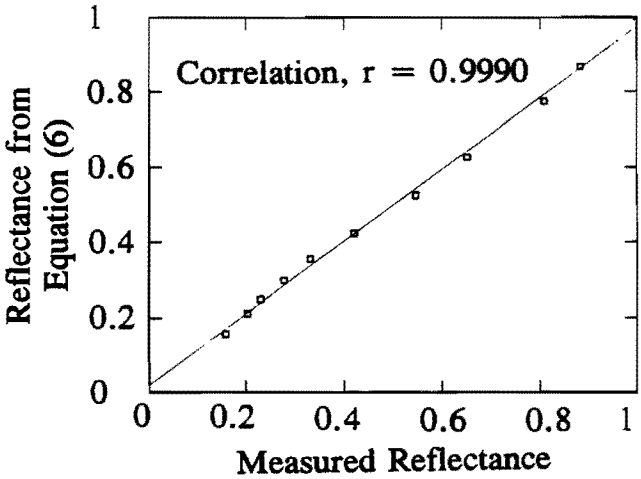

Table I: Correlations between measured reflectance of R and three different models: Murray-Davies equation (1), Yule-Nielsen equation (2), and the modified Murray-Davies of equation (3).

Printing Process	Halftone Frequency, Lines/Inch	RMS Deviation from the Mean Reflectance Equation (1) Murray-Davies	Equation (2) Yule-Nielsen	n	Equation (3) New Model
Thermal transfer	65	0.063	0.020	1.45	0.016
ink jet	65	0.045	0.016	1.62	0.019
offset litho	65	0.026	0.019	1.60	0.024
offset litho	150	0.017	0.015	1.40	0.010

experimentally measured values of R, as shown in Figure (3). For comparison, R values calculated from the Yule-Nielsen equation are shown in Figure (4) versus the experimetnal values of R. In both cases, a figure of merit was determined by calculating the RMS deviation between the the experimental values of R and those calculated by either equation (2) or equation (3). This same experiment was repeated with halftone grey scales generated by several devices, and the results are summarized in Table I.

Modeling $R_i(F)$ and $R_p(F)$: Light Scattering

The data in Table I indicate equation (3) may indeed serve as a halftone model provided the individual components, $R_i(F)$ and $R_p(F)$, can be modeled. To develop an empirical model of $R_i(F)$ and of $R_p(F)$, we first examine the behavior of the ink and paper reflectance factors from image histograms as summarized, for example, in Figure (2). We note that R_i and R_p vary between limits as F_i varies from 0 to 1. It was typocally observed that the limit for R_i at $F_i = 0$ was the same as the limit for R_p at $F_i = 1$. It would seem reasonable this common limit would be the product of the reflectancd factor of the unprinted paper, R_g, times the transmittancy of the ink, T_i , at 100% dot. This behavior may be summarized empirically as follows.

$$R_g T_i \le R_p(F_i) \le R_g \quad \text{for} \quad 1 \le F_i \le 0$$

and

$$R_g T_i^2 \le R_i(F_i) \le R_g T_i \quad \text{for} \quad 1 \le F_i \le 0$$

Any of a variety of linear and non-linear functions might be written to model $R_i(F_i)$ and $R_p(F_i)$ between these limits. By trial and error, the following functions have been found to fit experimental data quite well.

$$R_i(F_i)=R_g T_i[1-(1-T_i)F_i^w] \tag{4}$$

$$R_p(F_p)=R_g[1-(1-T_i)(1-F_p^w)] \tag{5}$$

where $F_i = 1- F_p$

These functions contain two independently measurable parameters. These are the bulk reflectance of the paper, $R_g = R_p$ at $F_i= 0$, and the bulk transparency of the ink , $T_i=(R_i/R_g)^{1/2}$ for R_i measured at $F_i = 1$. These are analogous to the constants R_i and R_p in the Yule-Nielsen model. Also like the Yule-Nielsen model, an arbitrarily chosen power factor, w, is selected to provide the best fit to experimental data. The lines drawn in Figures (2), (5) and (6) illustrate the fit of equations (4) and (5) to experimental data from three different printing processes. In each case the index of fit was defined

Figure 4: Reflectance values calculated with the Yule-Nielsen equation versus measured values of macroscopic reflectance. The n value was chosen to maximize the correlation coefficient.

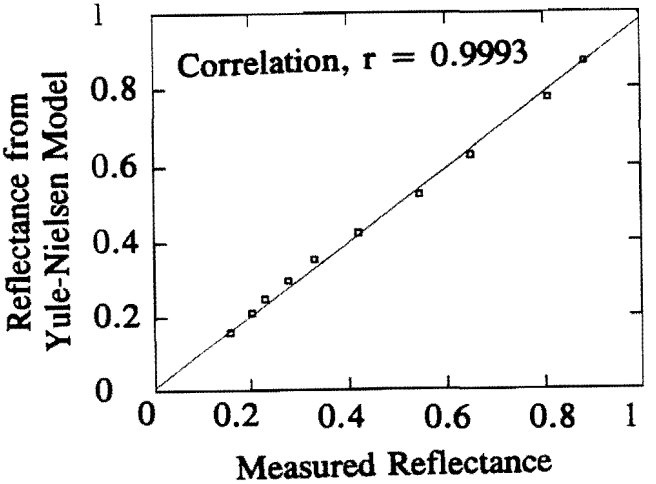

Figure 5: Thermal wax transfer data at 65 LPI. Reflectance versus Dot Area Fraction, F_i , for overall reflectance $R(F_i)$, ink reflectance $R_i(F_i)$, and reflectance of paper between the dots $R_p(F_i)$. $w = 0.443$

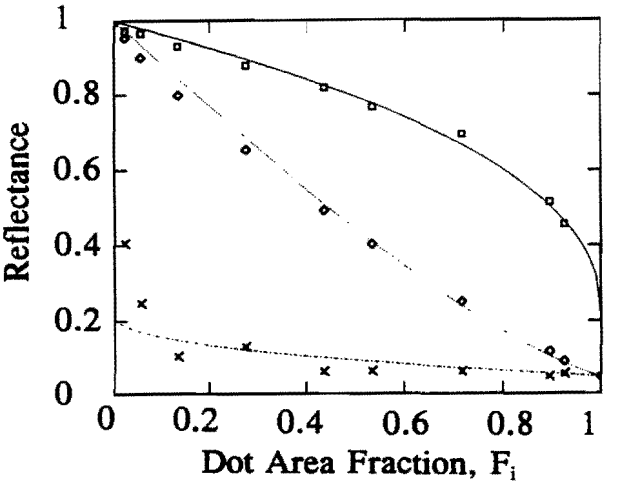

as the RMS deviation between the data points and the model. A single RMS deviation was calculated over both the $R_i(F_i)$ and the $R_p(F_i)$ data for a single index of fit. The same value of w was selected for both the $R_i(F_i)$ and the $R_p(F_i)$ data, and the value of w was selected to minimize the RMS deviation. An overall model of R versus F_i may then be achieved by combining equations (3), (4) and (5). With only the bulk constants, R_g and T_i, and the power factor, w, a reasonably close fit to the data is achieved, as shown in Figures (2), (5) and (6).

Modeling $R_i(F)$ and $R_p(F)$: Distribution of Transmittancy

The data in Figure (6) was generated from a 65 LPI halftone grey scale produced with an offset lithographic press. The same press, ink, and paper used to produce this data were used to print a 150 LPI halftone grey scale. Histogram analysis of the 150 LPI images resulted in the data shown in Figure (7). Clearly, the idea that R_i and R_p approach a common limit is not true in this case. The limiting values significantly overshoot each other. While several factors may contribute to this phenomenon, we would like to suggest a major contributing factor is the distribution of colorant, and thus transmittancy, in the ink dot. In other words, "soft dots", as well as light scatter, may contribute to the non-linearity of R versus F_i. This effect would cause very small dots to disappear as F_i approached zero. In order to account for this behavior, we would like to suggest substituting the product R_gT_i in equation (4) with a function which varies from R_gT_i to R_g as F_i varies from 1 to 0. The following model is proposed.

$$R_i(F_i)=R_g[1-(1-T_i)F_i^w]+[1-(1-T_i)F_i^v] \qquad (6)$$

Similarly, as F_i approaches unity, the paper between the dots may fill with colorant. If this occurs the apparent reflectance of the paper will decrease. In order to account for this behavior, we would like to suggest substituting R_g in equation (5) with a function which varies from R_g to R_gT_i as F_i varies from 0 to 1, or as Fp varies from 1 to 0. The following model is proposed .

$$R_p(F_p)=R_g[1-(1-T_i)(1-F_p^w)]+[1-(1-T_i)(1-F_p^v)] \qquad (7)$$

The power factor, v, may be thought of as a factor which models the softness of the dot edges. If v = 0, the dots are perfectly sharp and equations (6) and (7) reduce to (4) and (5). However, by adding this dot softness function to the model, the solid lines shown in Figure (7) result and provide a reasonable fit to the data.

Discussion

Figure 6: Offset lithographic halftone data at 65 LPI. Reflectance versus Dot Area Fraction, F_i , for overall reflectance $R(F_i)$, ink reflectance $R_i(F_i)$, and reflectance of paperbetween the dots $R_p(F_i)$. w = 0.225

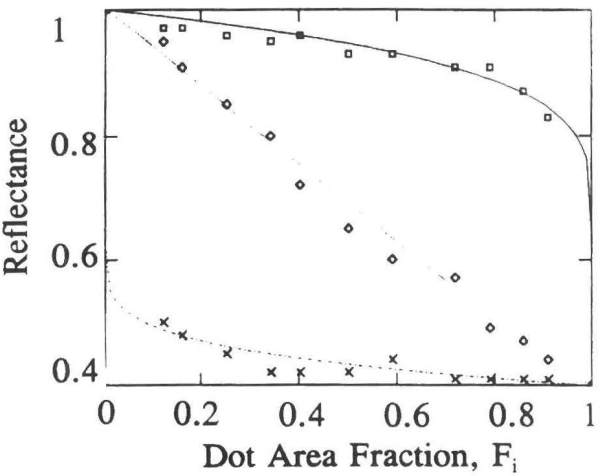

Figure 7: Offset lithographic halftone data at 150 LPI. Reflectance versus Dot Area Fraction, F_i , for overall reflectance $R(F_i)$, ink reflectance $R_i(F_i)$, and reflectance of paperbetween the dots $R_p(F_i)$. w = 0.357 and v = 0.30.

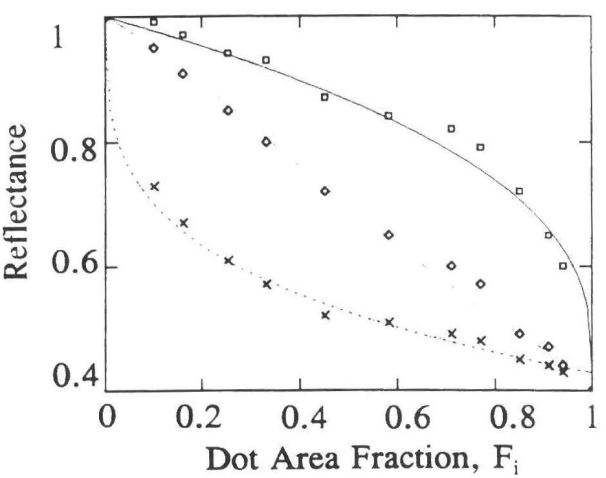

The values of n chosen to fit the Yule-Nielsen equation typically lie between 1 and 2. Pearson,[13] for example, suggests a mean value of 1.7 to fit most routine applications of the Yule-Nielsen function. Moreover, theoretical analysis suggests $n = 2$ is a limit unless factors other than the optical scattering of light are involved.[11] Both w and v in the model suggested by equations (3), (6) and (7) are limited to the range 0 to 1 by the empirical arguments from which the equations were derived. If one compares the behavior of the Yule-Nielsen equation with equations (3), (6) and (7), it is easy to demonstrate the two models are numerically identical under some, but not all, conditions. For example, both models reduce to Murray-Davies at $n = 1$ and at $w = v = 0$. Moreover, the new model produces numerically identical results to Yule-Nielsen at $n = 2$ when either w or v is unit. However, at intermediate values of n, w, and v, the two models do not produce identical numerical results at every value of F_i . It may be possible, therefore, to observe a better fit of one model over another provided experimental error can be reduced sufficiently to detect the difference between the models. Thus far, the experimental variability in the data we have generated is insufficient to distinguish the two models.

The new model, with constants w and v, has a disadvantage over the Yule-Nielsen model in that it is more complex to apply and does not provide a clear advantage to fitting R versus F_i data. The new model does, however, provide a description of some features of the image microstructure. That is, $R_i(F)$ and $R_p(F)$ are also modeled. Moreover, two different effects, the light scattering effect and the dot shape effect, are separately modeled. Unfortunately, the functions which model dot shape and scattering are identical, and this leads to some ambiguity. Based solely on R, R_i and R_p data versus F_i , one can not unambiguously distinguish between scattering and dot shape effects. While the model can be compared directly with experimentally observed values of $R_i(F)$ and $R_p(F)$, experimentally measured dot profiles of T_i , or of mean dot T_i versus F_i have not been achieved. Such additional image microstructure information would be of considerable interest in further developing the model. Nevertheless, the current model does preserve the linearity of photon additivity and is offered as an incremental advance in both the experimental and theoretical underastanding of the optical properties of ink-on-paper images.

Appendix: Experimental Procedures

Image Capture and Reflectance Calibration: The images in this study were captured with a Model 4810 CCD camera (COHU Electronics, San Diego, CA) onto a VISONplus-AT OFG frame grabber (Imaging Tech. Inc., Bedford, MA) in a 486/50/DX2 type PC. The frame grabber and camera were controlled by IMLAB software (Warner Frei, Santa Monica, CA). The image field of view was 2.50 mm by 2.26 mm, and the image was digitized at a pixel resolution of 512 by 462. Image analysis was accomplished with software routines developed by the authors, and the IMLAB software provided an

available and convenient shell for writing and running the programs. Illumination was achieved with a ring fiber optic illuminator attached to the microscope objective. As shown previously [14] the pixel values from the camera used in this work are linear with respect to the reflectance factor of the object being imaged. Pixel values were translated into reflectance factors by calibration against a dark frame, captured with the lens cap in place, and against a white reference. In all cases, the white reference was an unprinted region of the paper itself. Thus, reflectance values reported in this project are all relative to the reflectance of the paper substrate. Except for the stochastic grey scales, the same paper was used for all experiments. The paper was a coated sheet with a measured visual reflectance of 0.87.

Calculation of Fractional Dot Area, F_i : Once the image was captured and calibrated, it was displayed on a relative pixel scale of 0 to 255, corresponding to a reflectance range of 0 to 1. Histograms were calculated from these images, but data is reported in terms of reflectance rather than pixel value. Software line scans were carried out across several lines of dots. The transition point between dot and paper was defined as the region of maximum rate of change in pixel value, dR/dx, in moving from the center of a dot (Rmin) to the center of the paper (Rmax). The value of R at this maximum gradient was selected as the "threshold value", R_t. An average of several line scans across several dots was used. The value of F_i was then determined by integrating the image histogram up to the mean value of R_t.

Halftone Samples : With the exception of the stochastic grey scale, all halftones were printed on the same coated paper stock. Offset lithographic images were printed by the RIT T&E center using oil based ink. Thermal transfer and ink jet images were printed by the RIT Research Corporation on proprietary, laboratory machines. The thermal transfer engine was a CalComp 6603-XF, capable of 300 DPI resolution, with a thermal wax transfer ribbon. The ink jet was a Canon BJC-600, bubble-jet engine capable of 360 DPI resolution. The stochastic, or "FM" halftone grey scale was an UGRA Select Velvet screen generated with a Agfa Select Set 7000 image setter. The output screen tint was contact printed onto Kodak Quartz Contact Paper, a very high resolution, high contrast photographic print paper.

Acknowledgement

The authors would like to express their appreciation to the 3M Company for support of this project. Special thanks to Richard Fisch for encouragement and guidance in the directions and priorities of the project. Thanks also to Bruce Blom of Mead Central research for incouragement and advice.

Literature Cited

1. A. Murray, J. Franklin Inst., 221, 721(1936)

2. J.A. Yule and W.J. Nielsen, Tech. Assn. Graphic Arts (TAGA) Proc., p65 (1951)

3. J.A.S. Viggiano, TAGA Proceedings, p. 647 (1985).

4. J.S. Harrington, TAGA Proceedings, p. 144 (1991)

5. Y. Shiraiwa and T. Mizuno, J. Imag. Sci. & Tech, 37, 385 (1993).

6. W.W. Pope, TAGA Proceedings, p. 142 (1989)

7. F.R. Clapper and J.A. Yule, J. Opt. Soc. Am., 43, 600 (1953)

8. F.P. Callahan, J. Opt. Soc. Amer. 42, 104 (1952)

9. J.A.C. Yule, D.J. Howe, and J.H. Altman, TAPPI, 50, 337 (1967)

10. F. Ruckdeschel and O.G. Hauser, Applied Optics, 17, 3376 (1978)

11. J.R. Huntsman, J. Imag. Tech. 13, 136 (1987)

12. M. Pearson, TAGA Proceedings, p. 415 (1980)

13. J.S. Arney and D. Stewart, J. Imag. Sci. & Tech., 37, 504 (1993)